Spectral filtering with diffractive reflection gratings for fast superconducting detectors in the THz frequency range

Journal of Physics: Conference Series **1559** (2020) 012017 doi:10.1088/1742-6596/1559/1/012017

Spectral filtering with diffractive reflection gratings for fast superconducting detectors in the THz frequency range

A Schmid[1], A Kuzmin[1], S Wuensch[1], K Ilin[1], E Bruendermann[2], D Scherhaufer[3], A-S Mueller[2] and M Siegel[1]

[1]Institute of Micro- and Nanoelectronic Systems (IMS), Karlsruhe Institute of Technology (KIT), Hertzstrasse 16, 76187 Karlsruhe, Germany
[2]Institute for Beam Physics and Technology (IBPT), Karlsruhe Institute of Technology (KIT), Hermann-von-Helmholtz-Platz 1, 76344 Eggenstein-Leopoldshafen, Germany
[3]Institute for Micro Process Engineering (IMVT), Karlsruhe Institute of Technology (KIT), Hermann-von-Helmholtz-Platz 1, 76344 Eggenstein-Leopoldshafen, Germany

E-mail: alexander.schmid@kit.edu

Abstract.

In this work we describe the design process of a grating spectrometer with fast superconducting THz detectors based on Niobiumnitride. The main application is the use as a diagnostic tool for accelerator-based sources of THz radiation like synchrotrons, where interactions of the electron bunches in storage ring lead to fluctuations in spectrum and intensity of the emitted radiation.

Guidelines for the design of the two main parts, grating and detector design, are given. Here, a blazed reflection grating for a frequency range of 1 THz to 5 THz has been developed and successfully fabricated in a high-precision milling process out of brass. Also three different planar antenna designs (double-slot, annular slot and log-per spiral) in combination with quasi-optical bandpass filters for the THz range have been simulated and evaluated for best spectral resolution and power coupling.

Finally, we have verified grating performance for pulsed THz radiation of 1 THz in an experiment conducted at the synchrotron light source of the KIT. Excellent agreement of the grating performance to the simulations has been found.

1. Introduction

Superconducting antenna coupled hot-electron-bolometer (HEB) made from Niobium (Nb) and Niobiumnitride (NbN) have been used in the THz frequency range primarily as mixers in heterodyne receivers due to low noise and high sensitivity [1, 2, 3].

In recent years, NbN-HEB have found increasing interest as direct detectors for pulsed THz radiation at accelerator-based sources[4]. The fast response times make them a promising choice for longitudinal diagnostics of electron beams. As the spectrum of the emitted radiation is linked to bunch length and charge profile of the electron bunches in the storage ring[5, 6], the analysis of instabilities can make a large impact on accelerator research and development as well as application of THz radiation.

Although direct THz detectors allow easier setup than detection schemes like electro-optical sampling, the loss of phase information poses a challenge in the reconstruction of the original bunch profile. Here, detection schemes with spectral resolution in addition to fast response times would give more information. [7]

For frequencies below 1 THz, concepts for fast spectrometers and their application at accelerator light sources have been presented based on room-temperature Schottky diodes in a discrete setup [7] and on the high T_c superconductor Y-Ba-Cu-O in the form of an integrated array [8]. Both concepts share the need for careful adjustment of the THz optics to ensure reliable coupling of all detectors to the signal to be analyzed.

Once a staple of spectroscopy, grating spectrometers have been all but replaced by fourier-transform spectrometers for high-resolution applications. For fast spectroscopy they still offer a wide range of freedom in the design of a detection system. Also the single optical input port with a fixed position of all components are an advantage as far as coupling to the radiation signal is concerned. Given the advantages, we propose the design of a fast grating spectrometer with four NbN-HEB detectors in the frequency range of 1 THz to 5 THz as a tool for accelerator diagnostics.

Design of the grating in the THz range is the most challenging part in the design process. For frequencies below 1 THz different designs have been presented in the past: For example micromachined metal fourier gratings as power splitters in heterodyne mixers [9], as well as gratings made from pressure-molded [10] and additive-manufactured plastics [11, 12]. Above 1 THz, the smaller wavelengths require a higher quality of surface finish. We have designed a blazed reflection grating for 1 THz to 5 THz, that has then been fabricated in a high-precison milling process out of a brass substrate.

Design of the antenna-coupled detector forms the second part of the design process. We have evaluated three different antenna designs and compared them in regard to spectral resolution and coupling efficiency. As the detector chip is mounted on a dielectric immersion lens, we have chosen planar antenna designs that have been used successfully in the past: The double-slot antenna [8, 13, 14], the annular-slot antenna [15, 16, 17] and the log-spiral antenna [18, 19, 20], both alone and in combination with quasi-optical bandpass filters.

In order to verify the grating design, we have also performed an experiment at the synchrotron light source of the KIT.

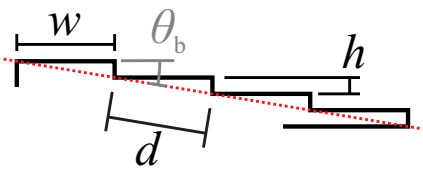

Figure 1. Sketch of the reflective blaze grating design. Individual steps are formed as right-angled triangles for easier fabrication.

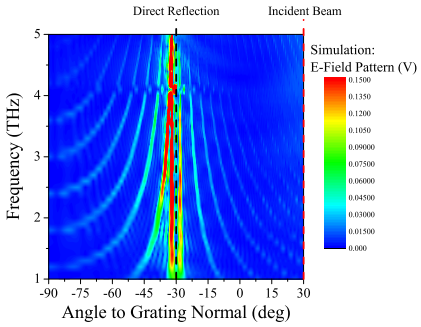

Figure 2. Simulation results of the grating design. The individual orders of diffraction are clearly visible.

2. Grating Design

Grating efficiency, i.e. the amount of power reflected into the different orders of diffraction is an important performance parameter of a diffractive grating. Especially the amount coupled to the higher order of diffraction as opposed to the specular reflection (0^{th}-order) can be maximized by using a blazed reflection grating [21]. The design parameters of a blazed grating are shown in Fig. 1. Here, a phase difference needed for diffraction is introduced by steps with a pitch of d. The angle of each step facet to the grating face normal is called the blaze angle θ_b. The step height h follows from facet width w and blaze angle θ_b. After [21] the grating efficiency for the first order of diffraction reaches a maximum when the blaze condition is fulfilled:

$$\lambda_b = 2dsin\theta_b \tag{1}$$

In case of the grating spectrometer scheme proposed in this work, some trade-offs have to be considered. First, the grating design can only be optimized for one wavelength due to (1). The grating is mounted in a fixed position with a fixed angle of incidence and can not be moved in the course of a measurement in order to achieve bunch-by-bunch resolution. Second, the grating has to be sufficiently effective for the whole frequency range under consideration. As signal intensity usually is weaker for higher frequencies we have optimized the grating design for the highest frequency under consideration, 5 THz.

The facet width has been fixed in a first step to $d \approx 1\ mm$ as this relatively large width allows for easier fabrication. This gives values of λ/d between 0.3 for 1 THz and 0.06 for 5 THz. In this ranges, the best grating efficiency in the first order is achieved by very low angles of θ_b[22]. The optimized design values for $\theta_b = 2°$ and an angle of incidence of 30°are then a pitch $d = 992.6\ \mu m$ resulting in a facet width $w = 992\ \mu m$ and a step height $h = 35\ \mu m$.

2.1. Simulations

In order to verify the design formulas, the developed grating design has been simulated with the electromagnetic simulation tool CST Microwave Studio (CST MWS)[1]. The grating has been modeled along the primary axis with 52 steps with width and height according to section 2.2 and a length of 20 mm along the secondary axis. Perfect electric conductor has been used as material for the grating and all boundarys of the simulation volume have been defined as open. The simulations were performed with the integral solver of CST MWS. A plane wave with the appropriate incident angle has been defined as the excitation source.

We have evaluated the diffraction introduced by the grating by defining farfield monitors in the frequency range of 1 THz to 5 THz in discrete frequency steps of 250 GHz. The resulting three-dimensional farfield-pattern of the electric field has then been evaluated along the azimuthal angle corresponding to the primary axis of the grating. The magnitude of the E-field pattern is plotted in Fig. 2 against angle to grating normal ϕ and frequency. The different orders of diffraction are clearly visible. Most prominent is the direct reflection at $\phi = -30°$ without any influence of diffraction. For higher order modes, the diffractive spread with frequency over angle ϕ introduced by the grating matches the values expected from the grating design formulas.

2.2. Fabrication

The grating design has been fabricated in a high-precision milling process developed at KIT-IMVT. A single-tip diamond turning tool is used in a computer-numerical controlled milling machine to achieve the high precision and accuracy needed for quasi-optical elements in the THz-range. The grating has been fabricated out of brass stock to a final length and width of

[1] www.cst.com

52 mm x 50.4 mm. After machining, the surface has been coated with a layer of magnetron-sputtered gold with a thickness of approx. 300 nm to protect against oxidation. Figure 3 shows a photograph of the grating after fabrication.

A result of a profilometric measurement of the surface roughness is shown in Fig. 4. The measurement stylus has been moved along the secondary axis of the grating. Thus, only deviation in surface quality due to machining and coating is visible and no step in the µm-range. The variations in the surface are periodic because the rotating turning tool is moved with a constant feed rate. Over a length of 100 m a maximum deviation in height of 230 nm has been measured. With a minimum wavelength of 60 µm for a frequency of 5 THz, this by far exceeds the requirements of surface quality for the frequency range under consideration.

3. Detector Design and Mode Order Sorting

High spectral resolution is the main requirement in a grating spectrometer. One of the main challenges here is illustrated by the simulation presented in section 2.1. Due to the periodical nature of the diffraction condition in the grating, multiples of the same frequency are reflected at the same angle for increasing order of diffraction. As an example, Fig. 5 shows the power pattern reflected from the grating at an angle of 42°. The data shown has been derived from the simulations presented in Fig. 2. Simulated data points are marked with a cross. The dashed line shows a fit as a guide to the eye. The angle shown coincides with the first-order maximum for a frequency of 1.5 THz and thus gives the angle of position for the 1.5 THz detector in the spectrometer. However, the same angle of reflection coincides with the second-order maximum for a frequency of 3 THz. Due to the grating design, the simulation shows the second-order mode is of comparable intensity for frequencies lower than 5 THz to the first-order mode and the spectral resolution is compromised.In order to suppress the unwanted higher modes, additional filtering has to be introduced between grating and detector, the so called mode order sorting.

In case of the antenna-coupled NbN-HEB at THz frequencies, the small size of the superconducting microbridge prohibits direct absorption of radiation. Thus the spectral resolution of the detector depends mostly on the antenna design. For the example of the 1.5 THz detector, we have performed simulations for three different antenna designs to be used with a silicon immersion lens and, in addition, quasi-optical filters. The results have been evaluated in regard to optimum suppression of high-order modes and best coupling efficiency and will be compared in section 3.5.

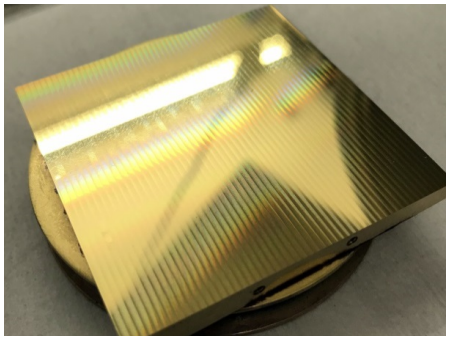

Figure 3. Photograph of the finished grating made from brass stock with a protective coating of magnetron sputtered gold.

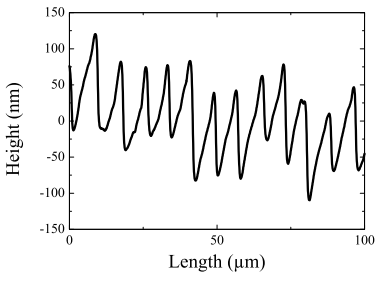

Figure 4. Profilometric measurement of the surface roughness of a single step of the grating.

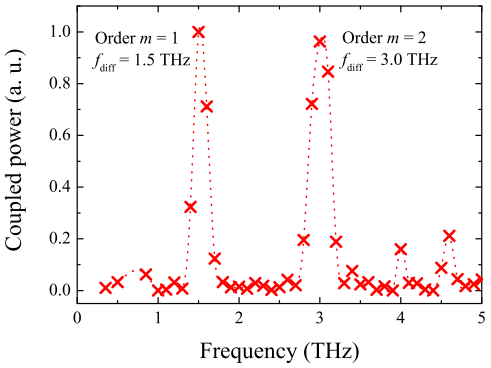

Figure 5. Simulation of the amount of power reflected by the grating at different frequencies for an angle of reflection of 42°. This angle coincides with the first-order maximum for a frequency of 1.5 THz. The presence of the second-order maximum at 3 THz makes the challenge of mode order sorting evident. Additional filtering is needed to suppress the signal from the unwanted mode.

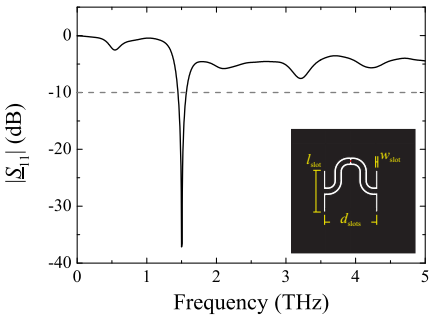

Figure 6. Simulated reflection parameter S_{11} of the double-slot antenna design (inset) for 1.5 THz. The antenna metallization is shown in black. The narrowband response is clearly visible.

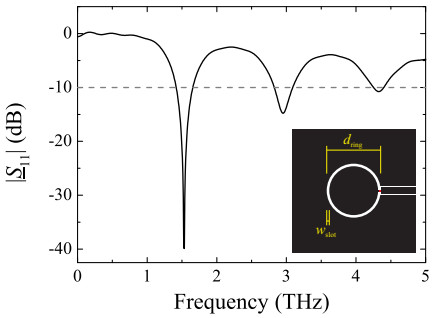

Figure 7. Simulated reflection parameter S_{11} of the annular-slot antenna design (inset) for 1.5 THz with a narrowband resonant response.

3.1. Double-slot antenna

The classical double-slot antenna has been simulated in a high-impedance version of the design (Fig.6 inset): A length of $\lambda_{guided}/2$ has been chosen for the two slots spaced approx. the same distance apart. This results in a high impedance at the feed point. The two slots are connected in series to the detector microbridge with two coplanar waveguides with a length of $\lambda_{guided}/2$ each. No impedance transformation is introduced for the design frequency resulting in a real antenna impedance of 300 Ω at the position of the detector bridge. Further information regarding the antenna design process can be found in [8]. For 1.5 THz the optimized design has a slot length $l_{slot} = 38.2\ \mu m$, a slot width $w_{slot} = 2\ \mu m$ and a slot spacing $d_{slots} = 47.7\ \mu m$. The double-slot antenna is linearly polarized and literature shows good coupling to Gaussian beams[23].

Figure 6 shows the simulated reflection parameter $|S_{11}|$ for the double-slot antenna. A very good match is achieved at the design frequency with a very narrow bandwidth. At a frequency of 3 THz the reflection is higher then -10 dB.

3.2. Annular slot antenna

The annular slot (or ring-slot) antenna (Fig. 7 inset) is a narrowband antenna like the double-slot antenna. The circumference of the annular slot is approx. λ_{guided}. The width of the slot

is much smaller than the wavelength thus leading to a first resonance frequency with a purely real impedance at the position of the detector bridge in the slot of 150 Ω. As with the double-slot antenna, the annular slot antennas is polarized linearly. Optimized antenna parameters for 1.5 THz are a diameter of the antenna of $d_{ring} = 31.6\ \mu m$ and a slot width $w_{slot} = 1.5\ \mu m$.

The simulated reflection parameter $|S_{11}|$ is shown in Fig. 7 and exhibits narrowband characteristics similar to the double-slot antenna with good matching at the design frequency. The higher harmonic resonances are better matched than in case of the double-slot antenna. At 3 THz and 4.5 THz the reflections are lower than -10 dB. The simulations results lead to the expectation of a inferior filtering performance of the annular-slot antenna compared to the double-slot design.

3.3. Log-spiral antenna

The log-spiral antenna (Fig. 8 inset) belongs to the group of frequency-independent wideband antennas. In comparison to the antennas in sections 3.1 and 3.2 the design is not the complementary slot variation. Here the receiving aperture is the metallization layer. Also the log-spiral antenna is mainly circularly polarized.

For the log-spiral antenna the three design parameters are the inner radius of the antenna $r_{inner} = d_{spiral}/2$, the progression factor of the spiral a_{spiral} and the number of turns n_{turns}. Additionally, a self-complimentary design has been chosen and it has been optimized to cover the whole frequency range under consideration of 1 THz to 5 THz. With the approximate formulas for lower and upper cutoff frequency given in [20], d_{spiral} is calculated to be 2.8 µm and D_{spiral} to 31.5 µm. This gives $r_{inner} = 1.4\ \mu m$, $a_{spiral} = 0.31$ and $n_{turns} = 1.5$.

Correspondingly, the simulated reflection parameter $|S_{11}|$ in Fig. 8 shows wideband behavior without any resonances and a lower cutoff frequency of approx. 1 THz. With $|S_{11,Min}| = -28\,dB$ the matching is not as good as in the other two antenna designs.

3.4. Quasi-optical band pass filters

Quasi-optical filters for the THz range are an additional possibility to filter the signal reflected from the grating. The filters are placed inside the cryostat in front of the individual detector blocks holding the detector chip and the immersion lens. Figure 9 shows commercially available[2] band pass filters. These filters are made from a single layer of Nickel foil with holes engineered to

[2] http://www.tydexoptics.com/

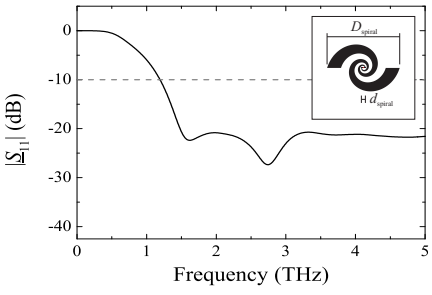

Figure 8. Simulated reflection parameter S_{11} of a log-spiral antenna design (inset). The antenna metallization is shown in black.

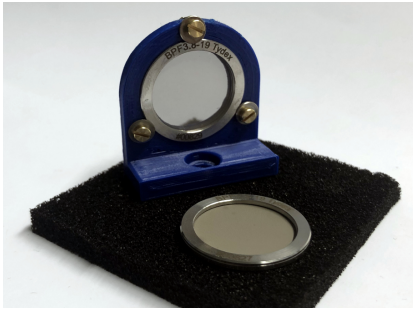

Figure 9. Commercial quasi-optical THz bandpass filters with holder. Clear aperture is 19 mm.

give the desired passband. The overall outer diameter of the filters used in this paper is 25 mm with a clear aperture of 19 mm. In case of the filter for a center frequency of 1.5 THz the filter introduces an transmission loss of 12.9%, a 3 dB-bandwidth of the passband of approx. 15% and an out-of-band attenuation of approx. 25 dB.

3.5. Comparison

The simulation results for the different antenna designs in sections 3.1-3.3 have been used to approximate the power coupled to the detector bridge for an angle of reflection of 42° (c.f. Fig. 5). The signal reflected by the grating was assumed to be linearly polarized. Coupling losses between the Gaussian mode after the grating and the immersion lens with the antenna as well as reflection losses at the boundary from air to dielectric lens have been neglected. Impedance of the NbN microbridge was assumed to be 300 Ω due to bridge sizes and surface resistance used in detector fabrication.

Figure 10 a) shows the calculated power coupled to the detector microbridge for the three different antenna designs. The double-slot antenna exhibits the highest coupling at the design frequency exceeding 98 %. At the second resonance frequency, the coupling is attenuated approx. 30 %. The annular-slot antenna shows inferior coupling at the design frequency compared to the double-slot design due to the mismatch of antenna to detector impedance. Also the relative attenuation at the second resonant peak is smaller due to the more pronounced resonant behavior with less dampening at higher modes (c.f. Fig. 7). In case of the log-spiral antenna with its wideband characteristics, no spectral filtering is achieved in the antenna. Overall amount of coupled power is the lowest of all designs. The large impedance mismatch and coupling loss due to the circular polarization of the antenna are the main contributors here.

Of the three antennas, the double slot antenna achieves the best filtering performance at the second resonance frequency. However, for this antenna design, the calculated response curve still has to be considered kind of a worst-case approximation. Here, the assumption of no coupling loss between the diffracted beam from the grating and the antenna is difficult. Compared to the other two antenna designs, the two slots form a type of antenna array, where spacing and phase conditions of the array elements become important. For the second resonance peak, the

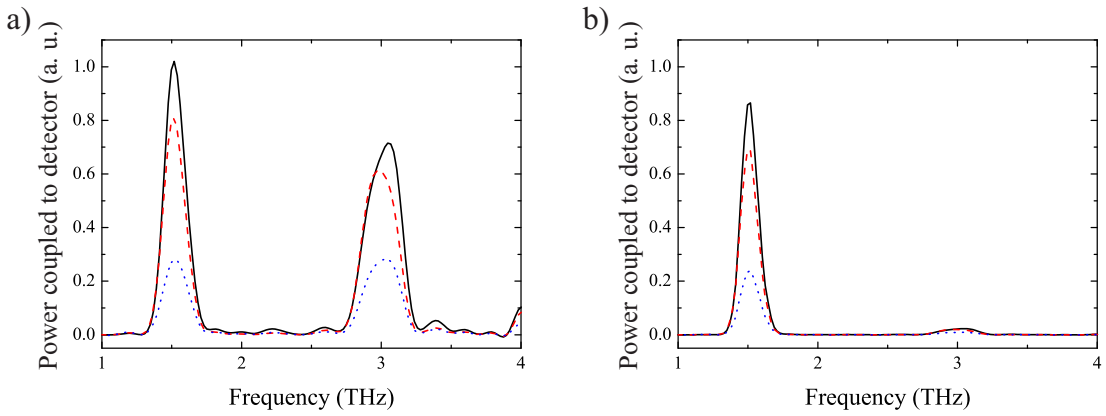

Figure 10. Calculated power coupled to the NbN detector for different antenna designs at the angle of reflection from the grating corresponding to the 1.5 THz maximum. a) Calculation for the three different antennas: Double-slot (solid), annular slot (dashed) and log-spiral (dotted). b) Calculation for the respective antennas with quasi-optical bandpass filter in front of the detector.

spacing is nearly λ_{guided} and the antenna farfield pattern develops considerable sidelobes along the substrate surface instead of the homogenous pattern at the design frequency [24]. Thus coupling is expected to be considerably lower in reality. On the other hand, the existence of strong sidelobes in this design makes the double-slot antenna not the preferred choice for a spectrometer without additional means of filtering.

As no sufficient filtering performance could been found with the three antenna designs alone, Fig. 10 b) shows calculations of the coupled power for the antenna designs with additional filtering by the quasi-optical THz bandpass filters introduced in section 3.4. The results show a attenuation of the signal at 3 THz of more than 95 % with an additional attenuation at 1.5 THz of approx. 13 %. Thus, a sufficient attenuation of signal from higher orders of diffraction (especially the second order in this configuration) can be achieved. Highest absolute coupled power is achieved with the double-slot antenna design due to being optimally matched to the assumed detector impedance.

4. Measurement of grating performance

A measurement of grating performance together with a NbN-HEB detector has been conducted at the IR2 Beamline[25] of the synchrotron light source of the KIT. The storage ring emits coherent synchrotron radiation in the THz range in a dedicated $low - \alpha_c$ mode[26]. A multi-bunch fill has been used in the experiment with a train of 33 bunches spaced 2 ns apart.

4.1. Experimental setup

Figure 11 shows a sketch of the experimental setup. The radiation from the storage ring is coupled out behind the main optics of the beamline through an optical window and then reflected 90° by a flat optical mirror. The spectral bandwidth of the radiation signal is then limited with a 1 THz bandpass filter. The grating is mounted with a kinematic optical holder and fixed to an incident angle of 30 ° in the blaze condition. A special rotary stage has been constructed in order to rotate a LHe cryostat with the NbN-HEB around the axis formed by the grating surface and the beam axis. Thus, the response of the detector could be measured for different angles of reflection. A detail photograph of the grating and the LHe cryostat can be found in Fig. 13.

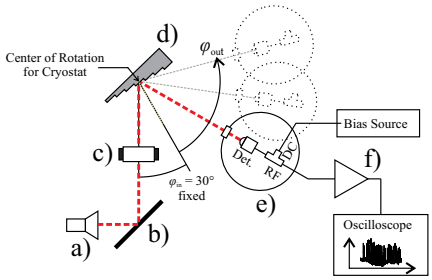

Figure 11. Sketch of the experimental setup: a) Optical window b) Flat mirror c) Quasi-optical bandpass filter for 1 THz d) Grating e) Cryostat on a rotary stage f) Amplifiers and oscilloscope

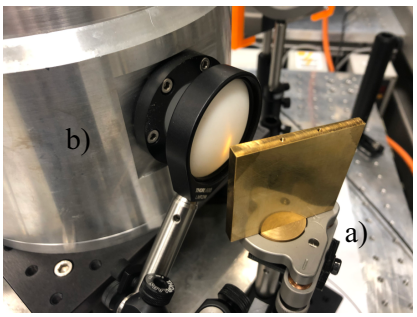

Figure 12. Detail photograph of the experimental setup with grating in kinematic optical mount (a) and LHe cryostat on rotary stage (b).

A NbN-HEB coupled to a log-spiral antenna (section 3.3) has been selected as detector sample. A bias voltage has been applied in the experiment over a cold bias-tee. The RF signal was then been read out over SMA-standard coaxial lines, amplified at room temperature and measured with a Agilent DSA-X93204A 33 GHz real-time oscilloscope.

4.2. Results

A complete train of pulses resulting from the multi-bunch filling pattern recorded with the NbN-HEB is shown in Fig. 13 a). Here, the angle of reflection was 30° and thus corresponds to the specular reflection. The signal from each bunch varies in amplitude due to the micro-bunching instability. Over time a shift in the baseline of the detector signal occurs. This can be attributed to a low-frequency cutoff in the RF readout path due to the bias-tee.

It is possible to fully resolve the radiation pulse emanating from each individual bunch in the pattern due to the fast response time of the detector. In Fig. 13 b) the detector response to an exemplary single bunch is shown in detail. A Gaussian function can be fitted with excellent fit to the rising edge of the signal. Deviation from Gaussian form in the falling edge is due to a weak bolometric tail. With a full-width-half-maximum of 105 ps the detector response is near the expected bandwidth limit in the readout chain.

In order to compare the measurement result to the calculations of the grating performance, the angle of the detector to the grating has been varied in intervals of 1°. At each position the detector signal has been averaged over 64 revolutions of the filling pattern in the storage ring. The normalized detector voltage has been plotted in Fig. 13 c) for each position together with the simulated grating response for a 1 THz signal. Up to an angle of 53°, where the body of the cryostat started to obstruct the beam path in the measurement setup, the results show excellent agreement between measurement and simulation.

5. Conclusions

In this paper, we have evaluated the performance of a diffractive reflection grating together with fast NbN-HEB detectors for the use in a grating spectrometer for the frequency range of 1 THz to 5 THz as a tool for acccelerator beam diagnostics. A grating design with perpendicular steps has been developed and fabricated in a high-precision milling process with a very good surface-finish quality out of brass. After application of a protective coating against oxidation of magnetron-sputtered gold, a surface roughness of 230 nm peak-peak has been achieved.

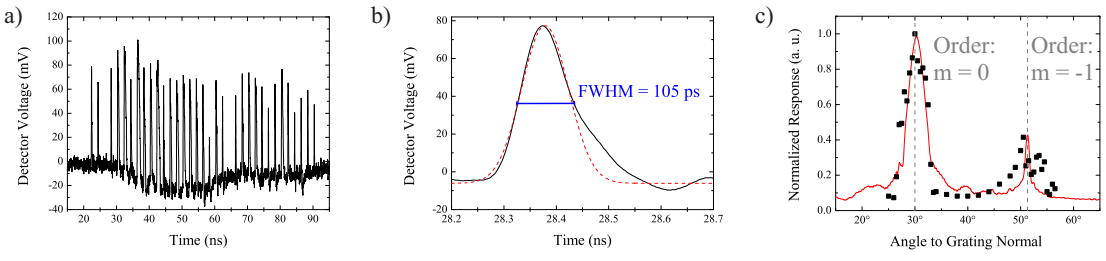

Figure 13. Measurement results: a) Train of pulses recorded at an angle of the detector to the grating normal of 30°(direct reflection). b) Example of a single pulse recorded in the experiment (solid line) and Gaussian fit (dashed). The NbN-HEB detectors shows a response time of 105 ps. c) Comparison of detector response at different angles to the grating (squares) and simulation results (solid line) for a frequency of 1 THz. The results show a good match.

Although the devloped grating design spreads the first order maxima of diffraction for the frequencies range under consideration over a 20° angle, thus allowing enough space for multiple detectors, the simulations showed unwanted overlap of higher orders of diffraction. In order to achieve high spectral resolution and mode order sorting, the three antenna configurations of double-slot, annular slot and log-spiral antenna together with commercial quasi-optical bandpass filters have been evaluated. Simulations have shown that in combination with the quasi-optical filters, all three antenna designs exhibit good spectral resolution while best power coupling is achieved for the double-slot antenna design.

The grating performance has been experimentally evaluated at the synchrotron light source of the KIT. The experimental setup allowed to measure detector response to the pulsed radiation emitted by the storage ring at a frequency of 1 THz for different angles to the grating surface. The observed response showed an excellent fit to expected response derived from simulations of the grating. The NbN-HEB detector with a log-spiral antenna used in the experiment exhibited a response time of 105 ps thus allowing to resolve the change in radiation emitted by individual bunches. These results are very promising for the construction of a multi-detector grating spectrometer based on the evaluated configuration. The two main requirements, single shot capability and spectral resolution are fulfilled.

Acknowledgments

A. Schmid and A. Kuzmin would especially like to thank H. Lambach und R. Dittmeyer of KIT-IMVT for their support in the fabrication of the grating. We would like to thank Y.-L. Mathis and the team of the IR beamlines at the synchrotron light source of the KIT for access to the beamlines and measurement support. A. Schmid would like to acknowledge the financial support by the Helmholtz International Research School for Teratronics (HIRST). This work was supported in part by BMBF contract number 05K16VKA.

References

[1] Bumble B and LeDuc H G 1997 *IEEE Transactions on Appiled Superconductivity* **7** 3560–3563 ISSN 10518223
[2] Yagoubov P, Kroug M, Merkel H, Kollberg E, Schubert J and Hübers H W 1999 *Superconductor Science and Technology* **12** 989–991 ISSN 0953-2048
[3] Cherednichenko S, Drakinskiy V, Berg T, Khosropanah P and Kollberg E 2008 *The Review of scientific instruments* **79** 034501 ISSN 0034-6748
[4] Hübers H W, Semenov A, Holldack K, Schade U, Wüstefeld G and Gol'tsman G 2005 *Applied Physics Letters* **87** 184103 ISSN 0003-6951
[5] Evain C, Barros J, Loulergue A, Tordeux M A, Nagaoka R, Labat M, Cassinari L, Creff G, Manceron L, Brubach J B, Roy P and Couprie M E 2012 *EPL (Europhysics Letters)* **98** 40006 ISSN 0295-5075
[6] Roussel E, Evain C, Szwaj C and Bielawski S 2014 *Physical Review Special Topics - Accelerators and Beams* **17** 9 ISSN 0031-2460
[7] Steinmann J L, Boltz T, Brosi M, Bründermann E, Caselle M, Kehrer B, Rota L, Schönfeldt P, Schuh M, Siegel M, Weber M and Müller A S 2018 *Physical Review Accelerators and Beams* **21** 9 ISSN 0031-2460
[8] Schmid A, Raasch J, Kuzmin A, Steinmann J L, Wuensch S, Arndt M, Siegel M, Muller A S, Cinque G and Frogley M D 2017 *IEEE Transactions on Appiled Superconductivity* **27** 1–5 ISSN 10518223
[9] Graf U U and Heyminck S 2001 *IEEE Transactions on Antennas and Propagation* **49** 542–546 ISSN 0018926X
[10] Busch S F, Born N, Koch M and Fischer B 2013 *Journal of Infrared, Millimeter, and Terahertz Waves* **34** 413–415 ISSN 1866-6892
[11] Busch S F, Weidenbach M, Balzer J C and Koch M 2016 *Journal of Infrared, Millimeter, and Terahertz Waves* **37** 303–307 ISSN 1866-6892
[12] Squires A D, Constable E and Lewis R A 2015 *Journal of Infrared, Millimeter, and Terahertz Waves* **36** 72–80 ISSN 1866-6892
[13] Filipovic D F, Gearhart S S and Rebeiz G M 1993 *IEEE Transactions on Microwave Theory and Techniques* **41** 1738–1749 ISSN 0018-9480
[14] Focardi P, McGrath W R and Neto A 2005 *IEEE Transactions on Microwave Theory and Techniques* **53** 1653–1661 ISSN 0018-9480

[15] Stephan K D, Camilleri N and Itoh T 1983 *IEEE Transactions on Microwave Theory and Techniques* **31** 164–170 ISSN 0018-9480
[16] Tong C E and Blundell R 1994 *IEEE Transactions on Antennas and Propagation* **42** 967–974 ISSN 0018926X
[17] Raman S and Rebeiz G M 1996 *IEEE Transactions on Antennas and Propagation* **44** 1438–1444 ISSN 0018926X
[18] Dyson J 1959 *IRE Transactions on Antennas and Propagation* **7** 181–187 ISSN 0096-1973
[19] Buttgenbach T H, Miller R E, Wengler M J, Watson D M and Phillips T G 1988 *IEEE Transactions on Microwave Theory and Techniques* **36** 1720–1726 ISSN 0018-9480
[20] Semenov A D, Richter H, Hubers H W, Gunther B, Smirnov A, Il'in K S, Siegel M and Karamarkovic J P 2007 *IEEE Transactions on Microwave Theory and Techniques* **55** 239–247 ISSN 0018-9480
[21] Palmer C A and Loewen E G 2002 *Diffraction grating handbook* vol 5 (Thermo RGL New York)
[22] Loewen E G, Nevière M and Maystre D 1977 *Applied optics* **16** 2711–2721 ISSN 1559-128X
[23] Vorst, MJM van der Integrated lens antennas for submillimetre-wave applications
[24] Brown G H 1937 *Proceedings of the IRE* **25** 78–145 ISSN 0096-8390
[25] Mathis Y L, Gasharova B and Moss D 2003 *Journal of biological physics* **29** 313–318 ISSN 0092-0606
[26] Muller A S, Birkel I, Gasharova B, Huttel E, Kubat R, Mathis Y L, Moss D A, Mexner W, Rossmanith R, Wuensch M, Wesolowski P, Perez F, Pont M and Hirschmugl C J 2005 Far infrared coherent synchrotron edge radiation at anka *2005 IEEE particle accelerator conference (PAC)* (IEEE) pp 2518–2520 ISBN 0-7803-8859-3